Dynamic Hazard Assessment for Slow-Moving Landslides using Persistent Scatter Interferometry in Antipolo

Luis Carlos S. Mabaquiao and Rosalie B. Reyes
Department of Geodetic Engineering, College of Engineering
University of the Philippines Diliman, Quezon City
Corresponding author: lsmabaquiao@up.edu.ph

Abstract – *Current landslide hazard assessment in the Philippines is done mainly using static base maps. The assessments are provided in the form of static landslide hazard maps. In this research, the technology of satellite interferometry in the form of Persistent Scatter Interferometry (PSI) is utilized in the City of Antipolo, Rizal to supplement the hazard maps by determining Persistent Scattering ground points exhibiting significantly higher velocities than a least-squares defined model. The study successfully detected 184,253 PS points using StaMPS. Assessment of the displacement of each point is done to isolate anomalous patterns by measuring both the actual displacement and the velocity of these PS points. The novelty of the study is the ability for periodic updating of anomalous points that facilitates the updating of landslide hazard maps every 12 days. Furthermore, the results of the study are overlain with published landslide susceptibility map to provide an additional dynamic layer that provides the movement of specific points and their corresponding classification at each image acquisition. The displacement was correlated to a stationary GNSS receiver having a correlation coefficient of 0.83 in the Line-of-Sight (LOS) direction suggesting the viability of the method in determining ground movement in aid of existing landslide hazard maps. Overall, the study demonstrates the feasibility of utilizing PSI in monitoring ground movement to complement conventional landslide hazard assessment in the Philippines.*

Keywords: Disaster, Interferometry; StaMPS; SARPROZ; RADAR

I. INTRODUCTION

1.1 Landslide Definition and Slope States

Landslides are defined as the movement of a mass of rock, debris, or earth down a slope under the influence of gravity [1]. This occurs when the resisting force of gravity and the frictional force are overcome by one another. In the context of slope stability, landslides are reactive processes that displace materials that have become unstable over time due to external forces, leading them to relocate until they achieve a stable state where forces are in equilibrium [2]. The binary classification of slopes into (1) stable and (2) unstable states is inadequate for studying landslides in the context of hazard assessment. Crozier [3] introduces a new classification of slope states to better comprehend slope stability behavior, categorizing them as (1) stable, (2) marginally stable, and (3) unstable states. In the context of hazard assessment, the transition from marginally stable to unstable slope state becomes a crucial phase for monitoring hazards. In this state, the slope is still considered stable, but single major events can trigger slope failure once a certain threshold magnitude is reached. Failure can be induced

Copyright 2023 | Philippine Engineering Journal

Phil. Eng'g J. 2023; 44(2): 59-87

by various external factors, including intense rainfall, earthquakes, and deforestation.

When states categorize a slope as static or in motion, this perspective is considered within the context of slope failure, which involves significant movement within the slope [4]. Movements that occur during the state transition from marginally stable to unstable are referred to as pre-failure movements. These movements may appear insignificant but serve as precursors that lead to slope failure [5]. The study aims to determine potential pre-failure movements by calculating the displacement of ground targets or Persistent Scattering (PS) Points. The movements of these points are analyzed to identify potential pre-failure indicators.

1.2. Landslide Hazard Assessment in the Philippines

Over the past 20 years, approximately 7,500 disaster events have been recorded by the Centre for Research on Epidemiology of Disasters (CRED) Emergency Event Database, with around 10% of these being landslides triggered by various sources [6]. From 1998 to 2017, the World Health Organization (WHO) has estimated approximately 18,000 deaths attributed to landslide events. The Philippines, situated in the Pacific Ring of Fire, has a history of experiencing landslide events. According to Petley [7], among 41 countries that were identified as key spots for landslides, the Philippines ranks 3rd in terms of casualties and recorded cases. Over the past two decades, the Philippines has documented at least ten (10) major landslide disasters that have resulted in more than 3,000 fatalities and reported over 2,000 missing persons [8].

In the local setting, Local government units (LGU) are tasked to develop the Comprehensive Land Use Plan (CLUP) and the Comprehensive Development Plan (CPD) as mandated by the Local Government Code (LGC). A key feature in the development of these plans is the integration of disaster mitigation with the prevailing hazards in the city or municipality. This includes the use of hazard maps, particularly landslide hazard, for municipalities and cities covering mountainous regions such as the city of Antipolo, Rizal. These maps show specific regions in the area where landslides are highly likely to occur. Several government agencies such as the Mines and Geosciences Bureau (MGB) and Philippine Institute for Volcanology and Seismology (PHIVOLCS) and research projects such as the Nationwide Operational Assessment of Hazard (NOAH) have published hazards maps to better aid in the local planning. However, the hazard maps currently utilized by the local government units are static in nature. These static maps seldom get updated and do not reflect the near real time movements within landslide susceptible areas. According to Brabb [9], at least 90% of landslide losses can be avoided if the problem is recognized before the landslide event.

1.3. Synthetic Aperture RADAR

Earth observation technology in the fields of satellite remote sensing and geographic information systems has proven to be an efficient and valuable tool for assessing natural hazards and their potential impacts [10]. In remote sensing, both optical and microwave remote sensors have been employed in landslide studies [11] to detect changes in land classification and measure minute movements between image acquisitions. This study explores the utilization of Synthetic Aperture RADAR (SAR) Remote Sensing, particularly Interferometric techniques, to generate hazard assessment layers with higher temporal resolution.

Interferometric SAR measurements allow the detection of deformations as small as millimeters between two (2) image acquisitions, and these deformations are crucial in identifying specific areas with the highest hazard potential [12].

Synthetic Aperture RADAR (SAR) is an active remote sensing sensor that operates in the microwave region of the electromagnetic spectrum. This microwave region is completely transparent to the atmosphere, and these microwaves do not interact with clouds, making SAR an all-weather remote sensing system [13, 14]. SAR Interferometry functions by detecting changes in range (the distance from the satellite to the target) through the phase information between two RADAR images acquired at the same location during different time periods, known as phase difference [15]. Figure 1 illustrates the geometry of Along-Track or Repeat Pass interferometry, where the change in the measured range (ΔR) can be determined from the phase difference between Antenna 1 and Antenna 2. In landslide hazard assessment, the change in the measured range is defined as the movement that occurred in the target area between the acquisition dates. Studies have found that using SAR Interferometry is useful in detecting landslides [12,40] and can be utilized with photogrammetric techniques to supplement emergency measures [10].
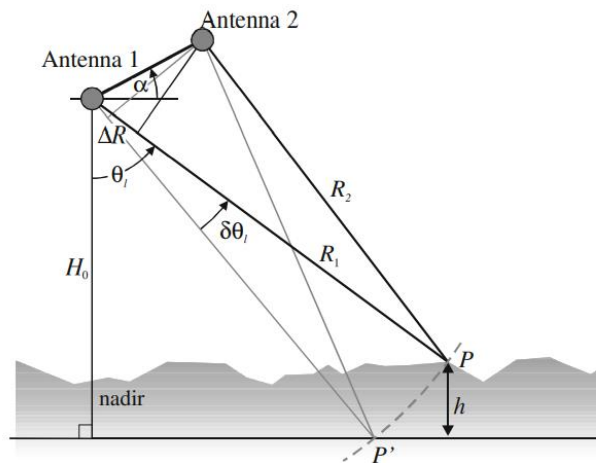

Figure 1. Along Track Interferometry [16]

1.4. Persistent Scatter Interferometry

The main disadvantage of using SAR Interferometry for landslide studies is the presence of interferometric pairs with low coherence values. This is mainly because majority of landslides are within non-urban areas, which tend to exhibit high noise values [17].

Persistent Scatter Interferometry (PSI) is an extension of SAR Interferometry that takes advantage of the capability of SAR images to be stacked into a time series analysis using a single master image as a reference [13]. This technique measures displacement values for each layer in the stack of co-registered images from selected PS points, which are points exhibiting stable phase behavior throughout the entire time span of the image stack [18]. PSI is a powerful tool used to measure minute changes in the Earth's topography by exploiting phase changes in each additional RADAR image within the stack [19]. It enables the measurement of

displacements in the study area, allowing us to assess the behavior of the PS points, including whether they are moving faster or conforming to a defined model. Two widely used approaches in PSI analysis are (1) the Temporal model approach using SARPROZ and (2) the Spatial Correlation approach using the Stanford Method for Persistent Scatterers (StaMPS). Similar studies have been done that utilizes the method of PSI in classifying landslides [41], expanding landslide inventory mapping [42], and landslide structural analysis [43].

PS points help determine the actual deformation rates of an area which is useful in the study of evaluating possible landslide areas by determining the pre-failure movement rates. PSI tracks the movement of PS points within the stacks of images and forms a deformation model [22]. In this study, two (2) methods of PSI in the form of SARPROZ [23] and StaMPS [24] will be utilized with both having different approaches in determining PS Points.

1.5. Objectives of the Study

In the study, PSI is used to identify PS points to detect potential pre-failure movements, which can ultimately lead to slope failure. The detected PS points serve as the actual ground target where displacement measurements are made. The derived displacements are analyzed and compared to a mathematically defined model to determine if the points are undergoing potential pre-failure movements during each image acquisition. This serves as the updatable spatial layer that supports the published landslide susceptibility map of the study area.

The aim of the study is to utilize a methodology that would support existing landslide hazard maps. The proposed methodology has the advantage of appending an additional updatable displacement layer to create a more robust and dynamic landslide hazard assessment through PSI. It is important to emphasize that this study does not seek to replace the existing hazard maps but rather intends to complement them through the utilization of satellite data.

II. MATERIALS AND METHODS

2.1. Study Area

Antipolo City is selected as the study area for this research. In August 1999, continuous rainfall led to a massive landslide in Cherry Hills Subdivision, resulting in the destruction of over 380 houses and the loss of at least 58 lives. The landslide engulfed the area in a mere 20 seconds [25]. According to a report by Calica [26], residents of Antipolo City have noted that flooding and landslides have been worsening due to the rapid population growth and the rapid development of subdivisions.

Antipolo is a city located in the Rizal province, Region 4A, Luzon, Philippines, covering an area of 306 square kilometers. According to the 2020 census, it has a population of 887,400 residents. The majority of the city is characterized by steep slopes, which makes it susceptible to landslides [25]. In addition to topographic considerations, various studies have analyzed landslide susceptibility in the city, providing the foundational static base layer for this study [27]. Project NOAH has classified a significant portion of the city as highly susceptible to landslides [34]. A study by Morales [35] also notes that the city of Antipolo is comprised of steep slopes making it prone to landslides. This underscores the importance of continuously

updating landslide hazard assessments to identify potential failure movements that could lead to disasters. Furthermore, the methodology employed in this study is intended to augment the LGU's existing disaster mitigation measures in place.
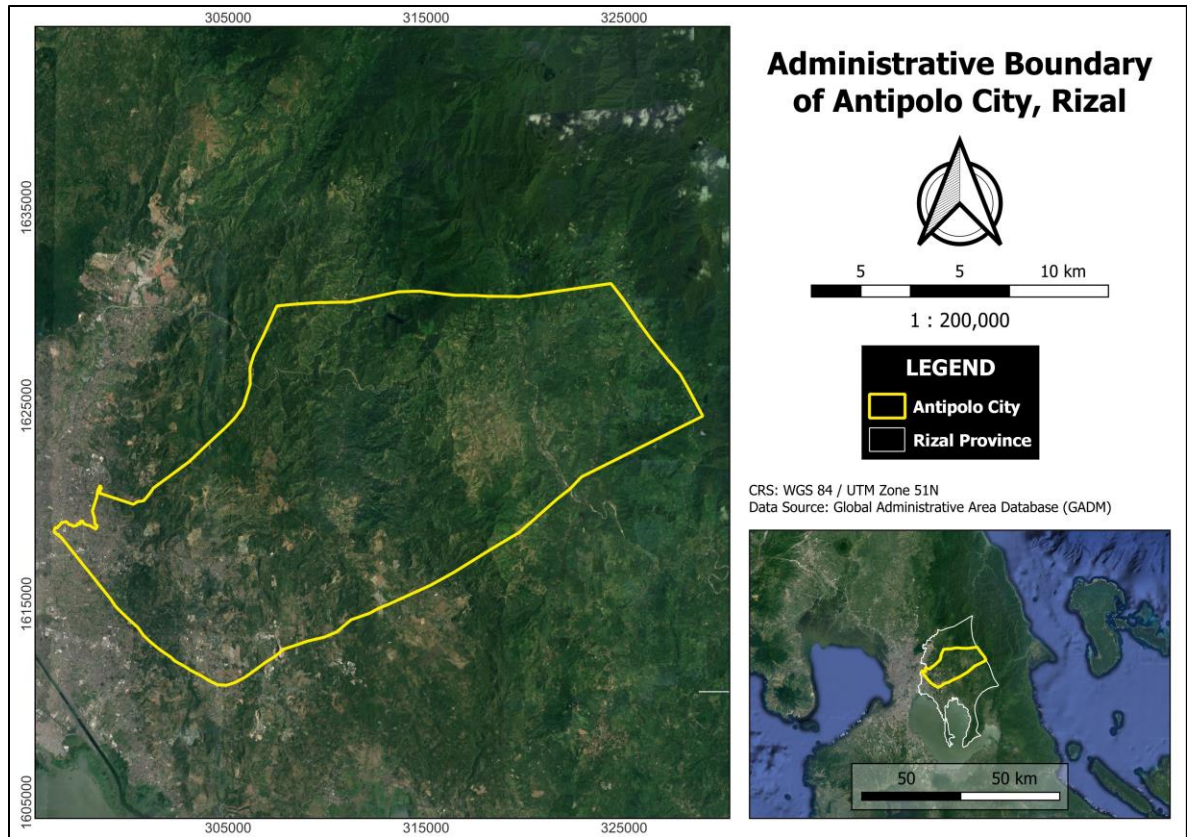

Figure 2. Antipolo City Administrative Boundary

2.2. Synthetic Aperture RADAR Images

Sentinel 1 is a dual-polarization radar satellite from the European Space Agency under the Copernicus Program. This satellite operates in the C band. Sentinel 1 has a temporal resolution of 12 days. It is best suited for interferometry due to its stringent orbit pattern [28]. A total of 30 Sentinel 1A Level 1 Single Look Complex (L1 SLC) SAR images will be captured at the same area with a temporal resolution of 12 days for a total of one-year analysis. Table 1 lists the acquisition dates of the SAR images used for the study.

Table 1. SAR S1A L1 SLC Acquisition Dates

Dates		
09 Jan. 2020	01 Jun. 2020	29 Sep. 2020
21 Jan. 2020	13 Jun. 2020	11 Oct. 2020
26 Feb. 2020	25 Jun. 2020	23 Oct. 2020
09 Mar. 2020	07 Jul. 2020	04 Nov. 2020
21 Mar. 2020	19 Jul. 2020	16 Nov. 2020
02 Apr. 2020	31 Jul. 2020	28 Nov. 2020
14 Apr. 2020	12 Aug. 2020	10 Dec. 2020
26 Apr. 2020	24 Aug. 2020	22 Dec. 2020
08 May 2020	05 Sep. 2020	03 Jan. 2021
20 May 2020	17 Sept. 2020	27 Jan. 2021

It can be seen that the dates for January to February had a considerable gap in the image dates. This was due to the unavailability of the data in same orbit in between the 2 dates. The selected dates were chosen to match the latest available yearly Global Navigation Satellite System (GNSS) data from the UP Base Station which will be used to evaluate the PSI displacement measurements.
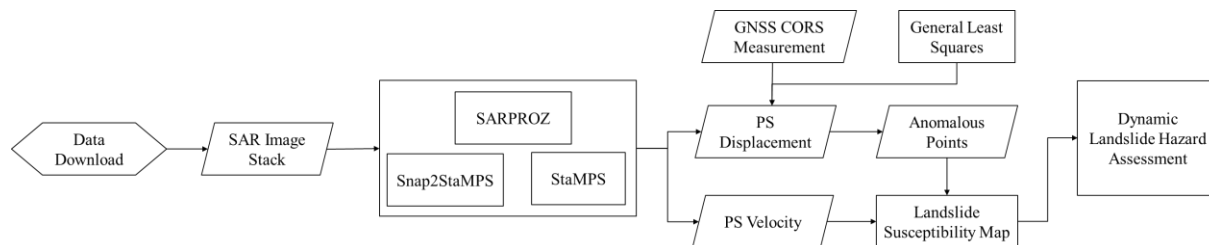

Figure 3. General Workflow

Figure 3 illustrates the overall workflow of the study. The process begins with the download of all necessary SAR data, which are then stacked together in preparation for PSI analysis. The stack is processed separately using SARPROZ and StaMPS. The resulting PS displacements and velocity values are analyzed to identify potential pre-failure movements through General Least Squares comparison. These displacement values are then compared to stationary GNSS measurements to determine the correlation. The obtained displacement, velocity, and anomalous points map are overlaid with the landslide susceptibility map to create the dynamic landslide hazard map. The detailed procedures for each step are discussed further in the succeeding sections.

2.3. SNAP2StaMPS Pre-Processing
The pre-processing of SAR images can be done manually via SNAP, but this method becomes time-consuming as more SAR images are stacked together. In this study, an

automated workflow for preprocessing is utilized. SNAP2StaMPS is a Python-based automated workflow that processes SAR L1 SLC images, making them ready for StaMPS ingestion. It comprises a set of graphs and Python codes to automate the processing chain for a single master interferogram PSI analysis [29].

2.3.1. Master Image Selection

The first step in PSI processing is the selection of the master image. This step aims to minimize the distribution of perpendicular baseline values, as a higher perpendicular baseline increases the likelihood of decorrelation or loss of coherence. In this study, the recommended master image is dated August 12, 2020. This particular date has been chosen as the master image for the PSI processing because it minimizes the baseline values among all combinations of the image stack. Only data from the IW 2 swath and VV polarization were used, as they provide higher backscatter compared to VH polarization.

2.3.2. Master and Slave Image Preparations

After determining the appropriate master image, it will undergo pre-processing along with the slave images. The objective of this step is to geometrically pre-process the master image, ensuring that the slave images match the properties of the master image for easier coregistration and interferogram generation. This is achieved by applying a precise orbit file and segmenting the master and slave images to align with the study area's location. This procedure is carried out to enable precise coregistration and stacking of each master-slave pair.

2.3.3. Image Coregistration and Interferogram Generation
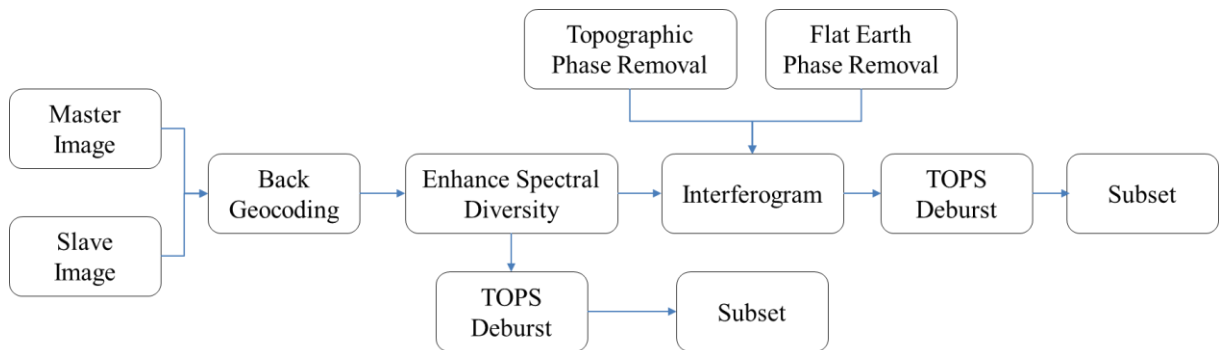

Figure 4. Coregistration and Interferogram Workflow

Figure 4 shows the workflow for this step. All preprocessed slave images will be coregistered with the master image. The process starts by back geocoding the master and slave image. This is accurately done because of the application of the orbit file. After the geocoding step, an Enhanced Spectral Diversity is applied. Afterwards the processing chain is split into 2.

The first process is debursting the coregistered image to remove the overlapping line in between bursts. The resulting product will be subset to the extents of the study area. The second process is the interferogram generation. In this step, an interferogram is computed between the

master and slave image. Along with the interferogram, both the flat earth and topographic phases are removed using an ellipsoid and a 1" SRTM DEM respectively. Debursting and sub setting is also applied to the interferograms.

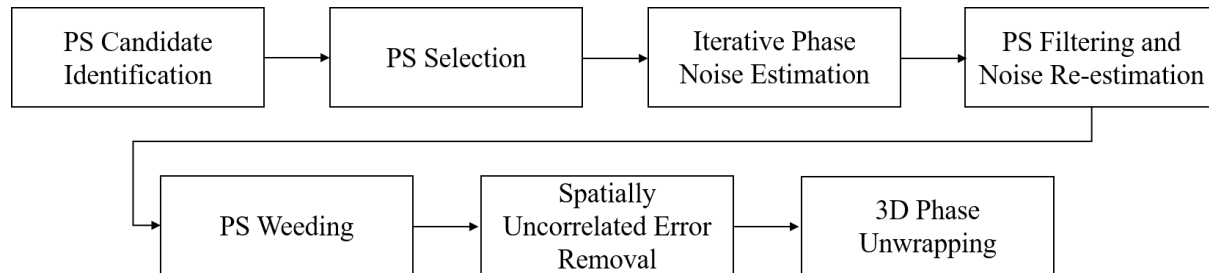## 2.4. Stanford Method for Persistent Scatterers (StaMPS)

Figure 5. StaMPS general workflow

StAMPS (see workflow in Figure 5) is an open research package based on MATLAB for PSI processing, developed by Hooper. This method is specifically designed for PSI applications in areas devoid of man-made structures, making it particularly valuable for landslide studies where built-up structures are often absent. The method utilizes both amplitude and phase measurements of individual pixels to determine their potential as PS points. It employs spatial correlation as an initial filter and does not rely on a linear deformation assumption for the PS points, rendering it suitable for areas characterized by non-linear deformation rates [30]. The goal of StaMPS is to isolate pixels that have a stable phase behavior and determine the movement of these pixels after filtering out all other candidates and use these pixels for phase analysis in determining the displacement and velocity measurements.

Initial candidate PS points are selected as candidates using the Amplitude Dispersion Index (D_A) due to the observed correlation between amplitude and phase noise for small values [20]. These selected points are used as candidates for subsequent phase analysis, from which displacement and velocity rates are derived. The candidate PS points exhibit stable amplitude measurements on the ground [21]. The Amplitude Dispersion Index (D_A) is computed as the ratio of the standard deviation of amplitude (σ_A) to the mean of a series of amplitude values (μ_A) in the stack of images (see equation 1). In StaMPS, the D_A serves as an initial filter for determining PS points.

$$D_A = \frac{\sigma_A}{\mu_A}$$
(1)

The usual range for this index for PSI processing is between 0.40 to 0.42 [28] up to 0.45 for largely vegetated areas [31]. For this study, the Amplitude Dispersion Index chosen is 0.45 due to the significant presence of vegetated areas in the study site.

The StaMPS workflow consists of seven general steps, as seen in Figure 5. The first step involves identifying candidate Persistent Scatterer (PS) points using the DA and loading these identified points. The subsequent step is an iterative process wherein the phase noise value is

estimated for each candidate PS pixel in every interferogram. This involves the combination and application of adaptive low-pass and band-pass filters, which effectively separate spatially correlated signals from the spatially uncorrelated ones [4]. In the following step, PS points are filtered and selected based on the phase noise values computed in the previous step. This process is repeated twice, as the re-estimation of phase noise becomes more accurate after spatially correlated phase contributions are removed. The selection process is then repeated. Next, PS weeding is performed. This step involves the removal of pixels selected in the previous step if they are attributed to signal contributions from neighboring ground resolution elements or if the pixel exhibit excessive noise. Afterwards, the spatially uncorrelated Digital Elevation Model (DEM) error is estimated and removed from the wrapped phase. Once these corrections have been applied, Phase Unwrapping is performed to determine the absolute cyclic differences in the interferograms. Phase Unwrapping results in the computation of displacements and velocities.

In the third step, the spatially correlated error is separated from the spatially uncorrelated error, with the latter being removed in the sixth step. After the phase unwrapping, errors associated with the orbit, spatially correlated errors, and master atmosphere are estimated in the final step. These estimated errors are then subtracted from the wrapped phase to obtain a smoother and more accurate unwrapped interferogram. To further refine the results, the last two steps are re-run to eliminate the estimated errors in the unwrapped interferogram and obtain a more precise estimate of these errors

2.5. SARPROZ

SARPROZ is a commercial software developed by Perrisin [23] with an intuitive user interface. The PSI method used by the program is based on the original Persistent Scatterer approach by Ferretti [19] and uses a Temporal Model for its PS processing. The same pre-processing is done similar to StaMPS where the master image is selected based on the perpendicular baseline values and each image is coregistered with the master image. The main difference between the 2 methods is the determination of the PS points. SARPROZ filters the initial candidate PS points by computing for the Amplitude Stability Index (S_A) (see equation 2) [23]. Unlike the D_A wherein the higher the value is specified, the more candidate PS points are selected, the inverse is true for S_A. For this index, the lower the value, the more points are initially selected as candidate PS points due to the more lenient criteria in filtering.

$$S_A = 1 - \frac{\sigma_A}{\mu_A} \tag{2}$$

The usual range of the S_A is 0.90 for highly urbanized, 0.80 for rural and up to 0.75 for vegetated areas [32]. In this study, 3 values for the S_A (0.85, 0.80, and 0.75) are used and explored in determining the number of PS points that will be generated for the study area in terms of number and distribution. The three values are chosen based the prevailing land cover in the study area.

After filtering the candidate points the remaining set of PS points are connected through a network using Delaunay Triangles. The software computes for the best GCP to use based on the stack of images. The GCP serves as the reference point for creation of the PS point network. The network ties and connects all detected PS points. From the network, it is assumed that the

contribution of the atmosphere between connected and nearby points are practically equivalent or varies only slightly over time. To model the phase contribution of the DEM and deformation, phase differences between points are obtained using a model, typically a steady-state or linear model. The estimation of deformation and DEM phase contributions is performed simultaneously. After acquiring the phase contributions, the parameters are obtained for each individual potential PS point and integrated using the least squares method. Atmospheric delays are estimated and subtracted from all potential points, and the process is iterated to determine the final set of PS points. It is important to note that the steady-state model used is assumed to be linear, implying that non-linear movements may not be fully described by this method. After the errors are removed, the PS points undergo phase unwrapping where the displacements and the velocity is computed.

2.6. Displacement Validation

The computed displacements from StAMPS and SARPROZ will be compared with the data from the GNSS station at Melchor Hall (UP Base Station – MMA 05) to assess the reliability of the derived measurements. Daily solutions for the entire year of 2020 are provided by the Coastal Sea Level Rise (CSLR) Project of the UP Training Center for Applied Geodesy and Photogrammetry (TCAGP). The vertical (up-down) measurements obtained from the GNSS will be converted to the Line of Sight (LOS) direction of the Radar Satellites using the incidence angle for a more accurate comparison [33]. The correlation between the trendlines of the displacement values will also be examined. The formula to convert the GNSS vertical measurements to SAR LOS is provided by equation 3.

$$GNSS_{LOS} = GNSS_{vertical} * \cos \theta_i \qquad (3)$$

where $GNSS_{vertical}$ is the measured vertical displacement of the GNSS station while Θi is the incidence angle of the radar sensor.

2.7. Anomalous Point Detection

Anomalous points are PS points that deviate from a General Least Squares (GLS)-based linear model up to a specified threshold. These points exhibit a higher-than-normal rate of movement, which increases the possibility of being pre-failure movements that are likely to evolve into slope failures. A moving average of 15 displacement measurements per point is used to create a linear model using the GLS criterion. This choice is based on the understanding that at least 15 interferograms are required to generate reliable PSI displacement measurements. Once the model is established, subsequent displacements are compared to the model to check if they fall within the expected 99% Confidence Interval (CI) threshold. If a displacement exceeds the threshold, it is considered an anomalous point.

This method is applied to all PS points to identify anomalous points within the image during a specific acquisition period. This process allows for the continuous updating of the GLS linear model to accommodate the latest displacement measurements. The initial computation utilizes displacements from 1 to 15 and compares them to the 16th measurement. Subsequent computations involve displacements from 2 to 16 compared with the 17th measurement, and so on, until the anomalous points are determined for the last acquisition date. This approach enables the updating of landslide hazard maps by identifying new sets of

anomalous points for each image acquisition.

2.8. Dynamic Landslide Hazard Assessment

The study's primary focus is on its ability to continuously update the landslide hazard map of the study area with each additional image acquisition. By combining the identification of anomalous points and the analysis of displacement measurements, an additional and updatable layer of hazard assessment is provided, highlighting areas where movements exceed the expectations set by the linear model. To provide a more localized context, the identified anomalous points are overlaid with the published landslide susceptibility map developed by Victor and Zarco [27], as depicted in Figure 6.

By combining these factors, local planning agencies can gain deeper insights into the movement of points and their classifications. These contributing factors are essential variables for prioritizing areas of focus when anticipating external environmental triggering events, such as heavy rainfall and other factors leading to slope failure and, ultimately, landslides. The objective of this study is not to replace the existing landslide hazard map of the study area but, rather, to provide an additional spatial measure that is updated every 12 days. This measure is intended to support the city's Disaster Risk Reduction and Management (DRRM) initiatives.
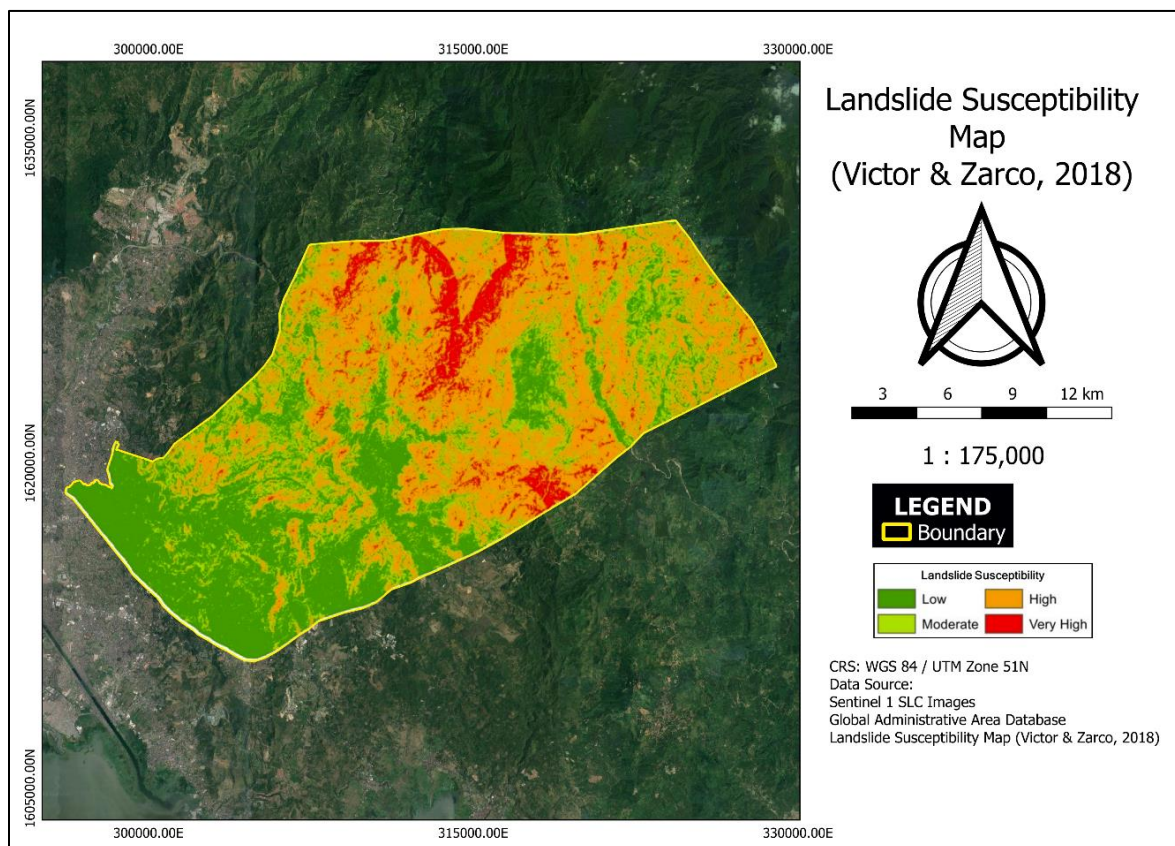

Figure 6. Landslide Susceptibility Map of Antipolo, Rizal [27]

IV. RESULTS AND DISCUSSION

4.1. SARPROZ

The original pre-processed images covered the majority of Metro Manila and some portions of the northern regions of Bulacan and the southern portions of Cavite. Subsequently, a bounding box was used to further limit the analysis to the designated study area. The detected PS points obtained using SARPROZ for the Metro Manila coverage are shown in Figure 7. Note that the figure is still in the RADAR coordinates thus the correct orientation has not yet been applied.

It is seen that the majority of the PS points are located in the lower half portion of figure 7, corresponding to Metro Manila and the city center of Antipolo City. This distribution is expected because urban areas primarily consist of stable phase scatterers in the form of man-made structures, such as built-up areas and buildings. These are targets that exhibit high coherence values since they are not expected to undergo any significant changes within the 1-year acquisition period. In the upper half portion of figure 7, the number of PS points drastically decreases, as this area corresponds to the mountainous regions of the study area, where fewer stable phase scatterers are expected.
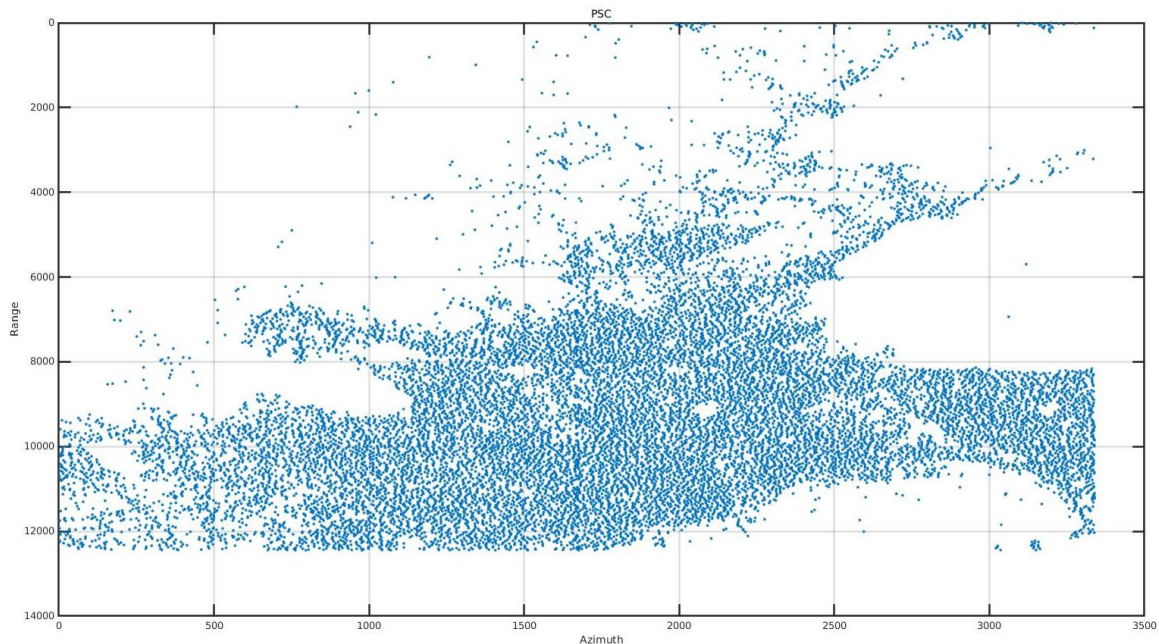

Figure 7. Detected PS Points using SARPROZ

Three (3) values for the S_A are used to densify the number of PS points; 0.85, 0.80, and 0.75. The shapefile of Antipolo City was used to clip the detected PS points to only within the boundary of study area. The specific SA values are chosen to determine which among the initial criteria would the detect the most PS points and where the detected PS point are.
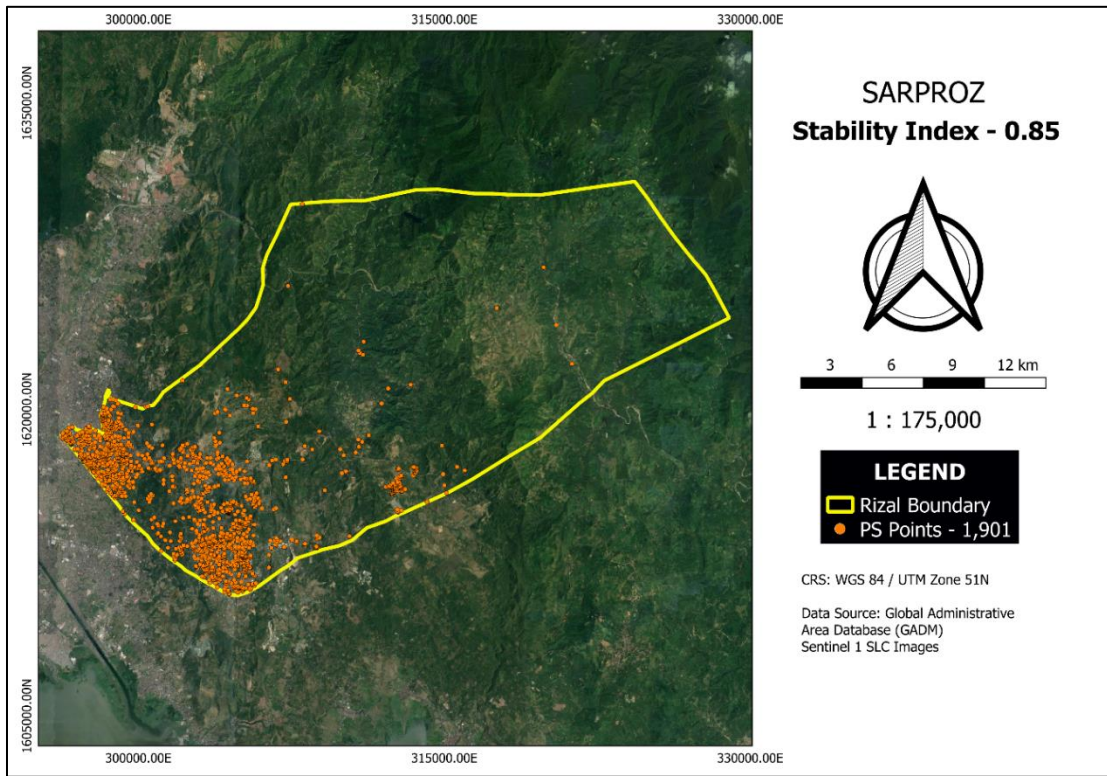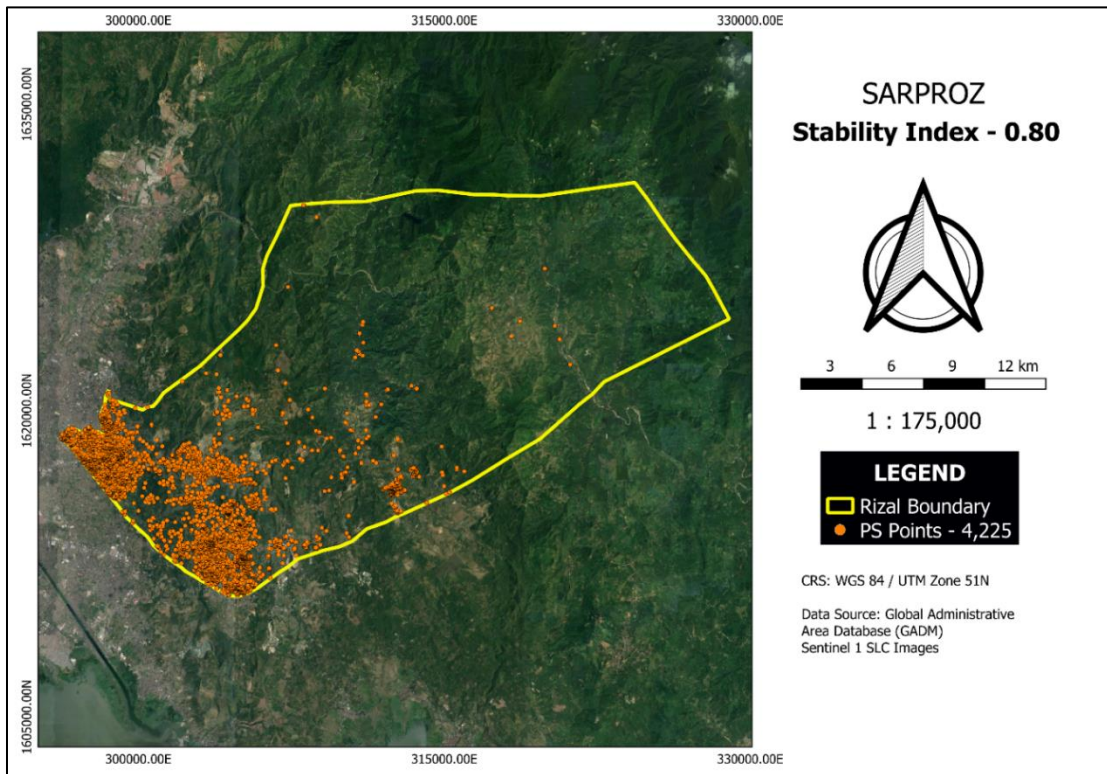
Figure 8. SARPROZ 0.85 S_A Value

Figure 9. SARPROZ 0.80 S_A Value

Figure 8 displays the detected PS points in Antipolo City using the S_A value of 0.85. A total of 1,901 PS points were identified. The majority of these points are concentrated within the urban areas of the city, primarily in the lower left portion of the figure. However, this distribution is not ideal for landslide hazard assessment, as very few PS points were detected in the upper right portion of the study area, which corresponds to the mountainous and vegetated region of the city where landslides are more likely to occur. To explore if increasing the S_A value would result in more PS points in the study, two additional values are tested. Figures 9 and 10 illustrate the PS points detected using S_A values of 0.80 and 0.75, respectively.

Using the SA value of 0.80, as seen in Figure 9, a total of 4,225 PS points were detected. Lowering the SA value to 0.75 resulted in the detection of 7,790 PS points as seen in Figure 10. Although reducing the SA value increased the number of PS points, the majority of them remain concentrated in high-urban areas. The analysis of displacement measurements in the mountainous region is limited due to the insufficiency of PS points in that area. Further lowering the SA value may theoretically increase the number of detected PS points but it would introduce more noise, making the retrieval of displacement measurements unreliable. A key limitation of the Persistent Scatterer approach by Ferretti [18] is its inability to detect PS points in areas devoid of man-made structures. This limitation is evident in the results, as high vegetated and mountainous areas have very few detected PS points. Consequently, the results of the SARPROZ processing were not used for further analysis in this study due to the lack of PS points, especially in the mountainous areas, which are of higher priority for landslide assessment.
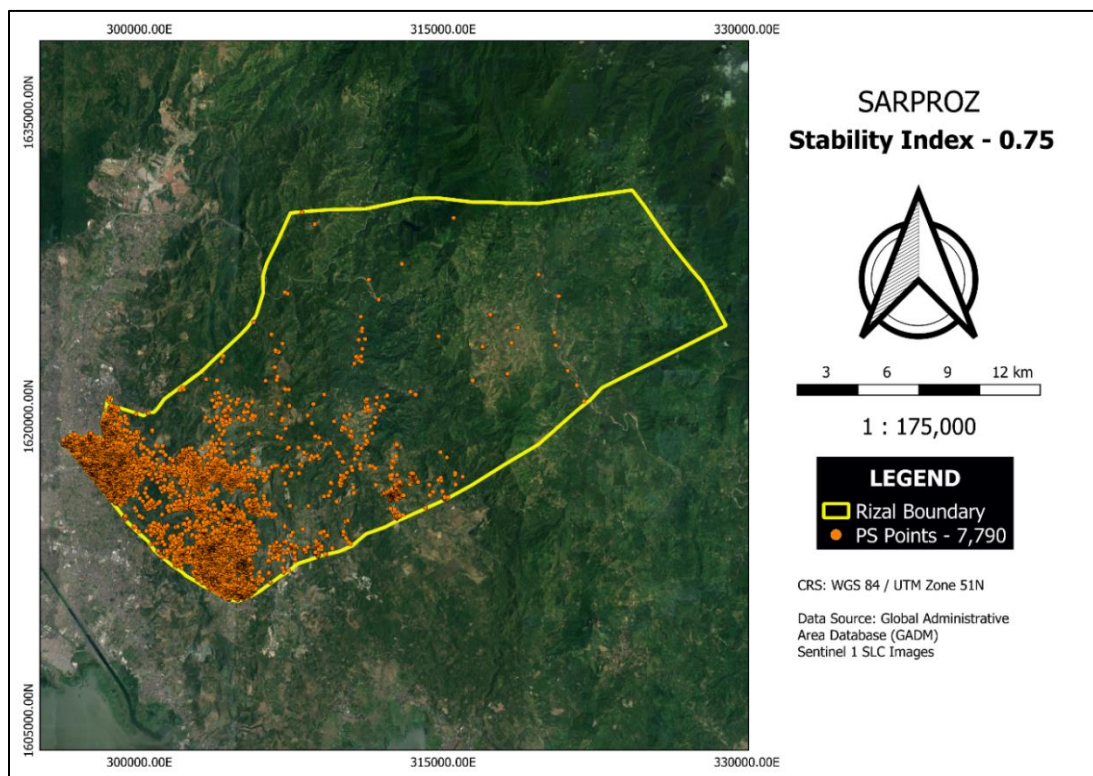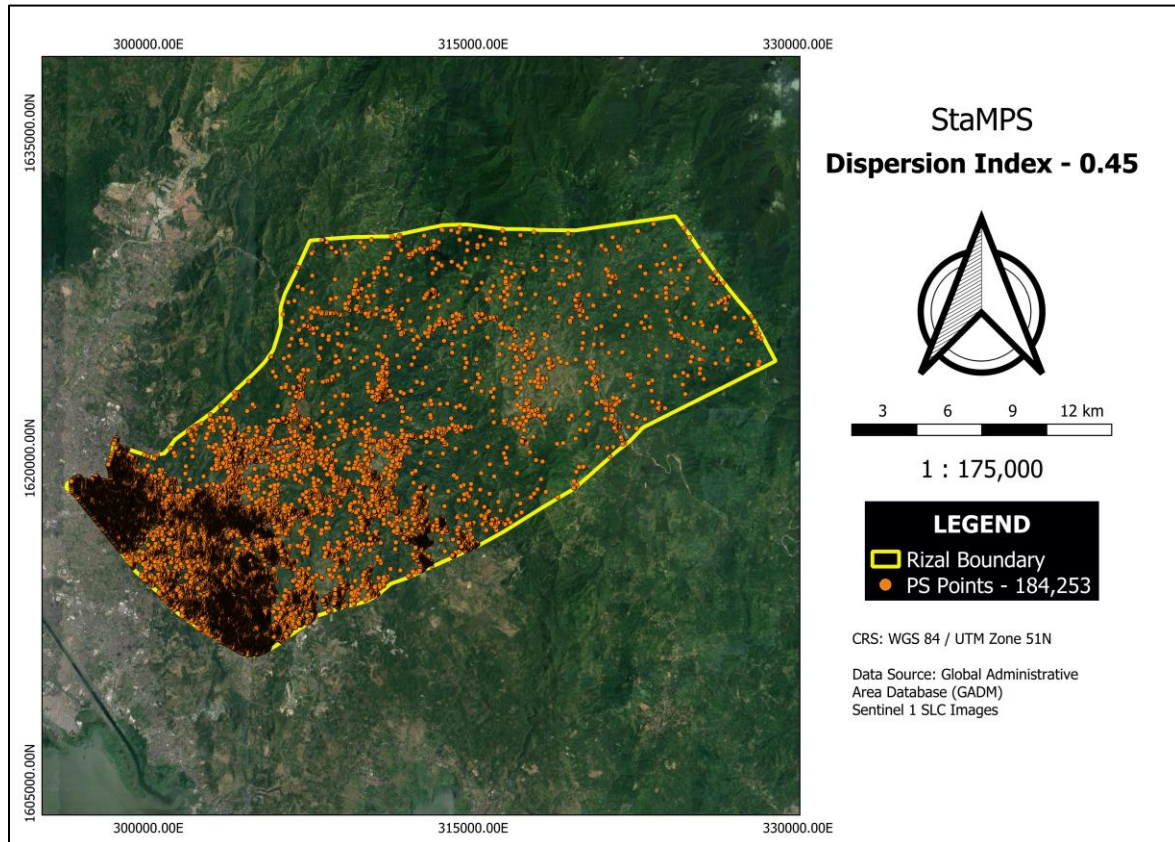
Figure 10. SARPROZ 0.75 S_A Value

4.2. StaMPS

A value of 0.45 was used for the D_A. The areas of Quezon city were included for the phase analysis of the UP Base station which will is used to verify the results of the measured displacements.

Figure 11. StaMPS PS Points (0.45 D_A)

The detected points were clipped in QGIS using the shapefile of the study area. Figure 11 displays the PS points within the study area. A total of 184,253 PS points were identified in the city of Antipolo alone. This significant increase in number can be attributed to the suitability of the StaMPS method, which was specifically developed for PS processing in areas devoid of man-made structures. From the same figure, it is evident that PS points are densely distributed in urban areas as seen in the south eastern portion of the figure. Simultaneously, a substantial number of PS points were detected in the vegetated and mountainous regions of the study area.

In the study, the results of the StaMPS processing are used to continue with the analysis, given the significant presence of PS points in vegetated and mountainous areas. These regions are of particular interest due to the potential for landslides, making continuous monitoring essential.

The one-year time span plays a critical role in determining the number of PS points to be identified in the study area. This specific timeframe was chosen to account for annual seasonal variations and any substantial changes within the study area. It ensures that PS points are not influenced by these variations, allowing us to select only those exhibiting a stable phase behavior over the course of one year. This criterion is important because any significant movement of a potential PS point throughout the entire data acquisition period can significantly impact the pixel's standard deviation over time. Consequently, such points are more likely to be filtered out during the initial processing using the D_A thus will not be detected as a PS point.
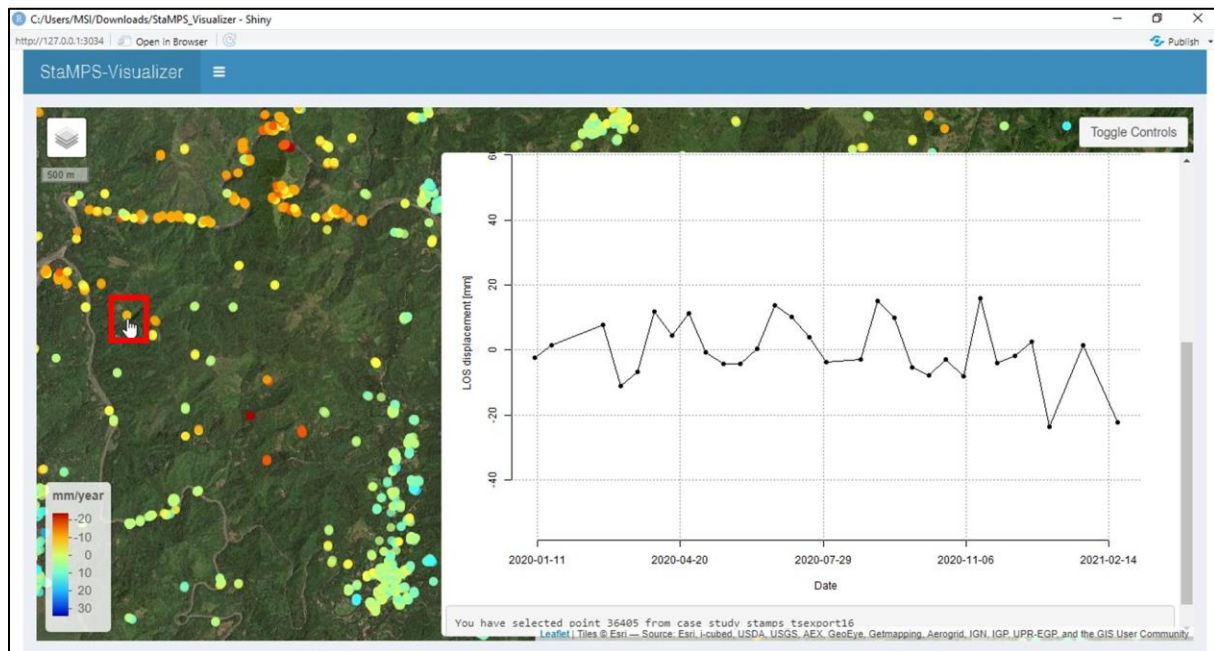

Figure 12. Sample StaMPS Visualizer

Figure 12 displays a selection of sample PS points within the study area. The graph on the right represents the displacement values of a sample PS point, measured in the LOS direction displacement, over a range of acquisition dates. This graph allows the observation of the trend in the movement of the PS points and identify dates on which significant movement occurred. Initial detection of potential pre-failure movements can be inferred using the graph with further analysis.

The velocity data is visualized in QGIS after clipping and filtering the PS points that fall outside the boundary of the study area. Figure 13 presents the velocity measurements obtained from the StaMPS processing within the study area.

The figure illustrates that the majority of urban areas in Antipolo City exhibit minimal movement, with the exception of the northwestern section of the city center, where a cluster of subsidence movement is seen. In the mountainous regions, the higher elevations at the center of the study area, which coincide with the highest elevation values, experience subsidence at a

rate of approximately 12mm/year. Conversely, the lower regions in the southeast show uplift with values around 22mm/year. These uplift and subsidence patterns may be linked to erosion and deposition processes in the upper mountainous areas as the slope state evolves over time.
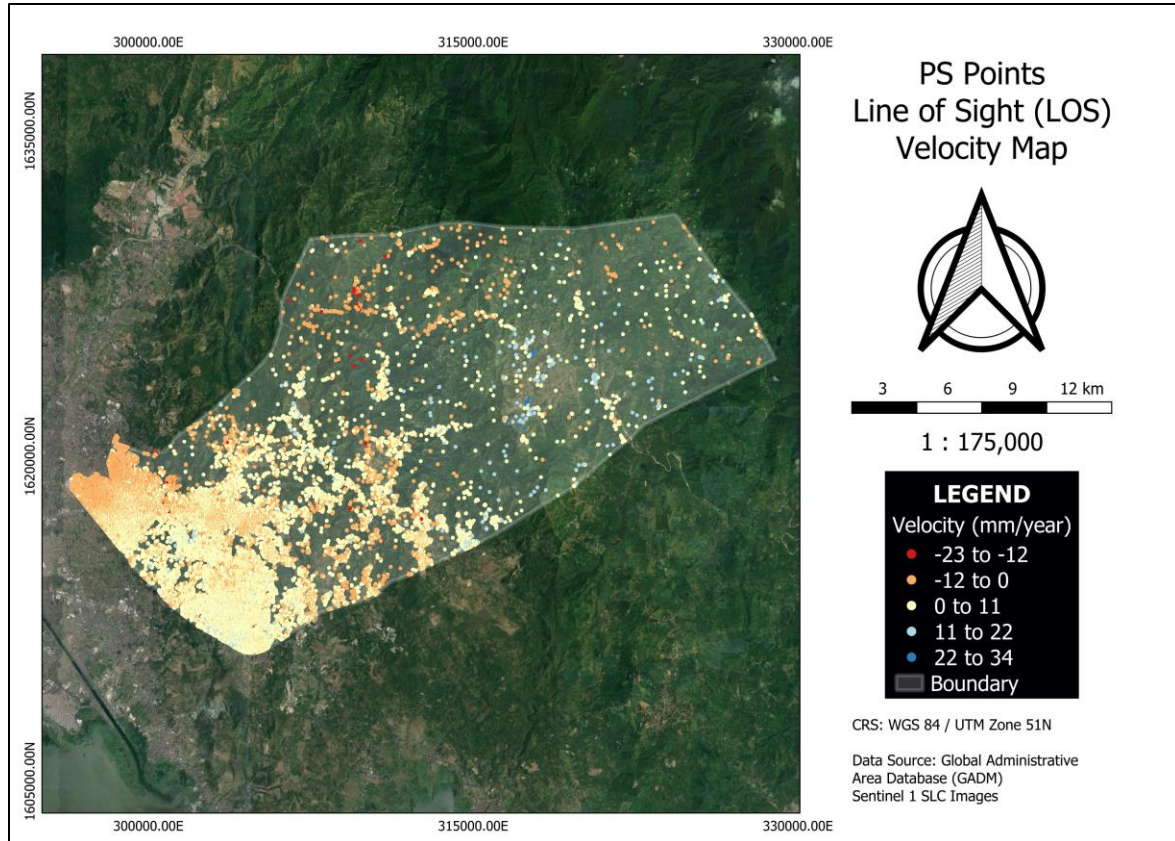

Figure 13. PS Points LOS Velocity

The outcome of the StaMPS processing have enabled the detection of movements within mountainous regions, through the identification of a substantial number of PS points. Aside from detection, it is possible to track the movement of PS points across multiple image acquisitions. Additionally, the calculation of velocity for the PS points enables the identification of areas experiencing significant changes in their movement rates.

These results offer valuable insights for local planning agencies, particularly with respect to areas at high risk of landslides, as indicated on published maps. The velocity map provides an overview of movement trends over a one-year timeframe. This information is instrumental for hazard management, aiding in preparedness and mitigation efforts. On the other hand, conducting further analysis of PS point movements is imperative for near real-time landslide hazard monitoring. This involves examining movements in greater depth and categorizing PS points with higher movement rates. The next subsection shows the results of the point classification.

4.3. Anomalous Points

In addition to the initial detection of PS points within the study area, a comprehensive analysis of their actual movements is undertaken to provide valuable insights for local planning agencies, particularly in prioritizing mitigation measures. This analysis involves the identification of anomalous points.

To identify these anomalous points, a linear model is generated using a general least squares approach, based on the first 15 displacement measurements for each PS point. Subsequently, each subsequent measurement is compared to the established model to check whether it falls within the 99% CI value. This rigorous method aids in determining areas that may require additional attention and prioritization for mitigation efforts during a specific acquisition date.
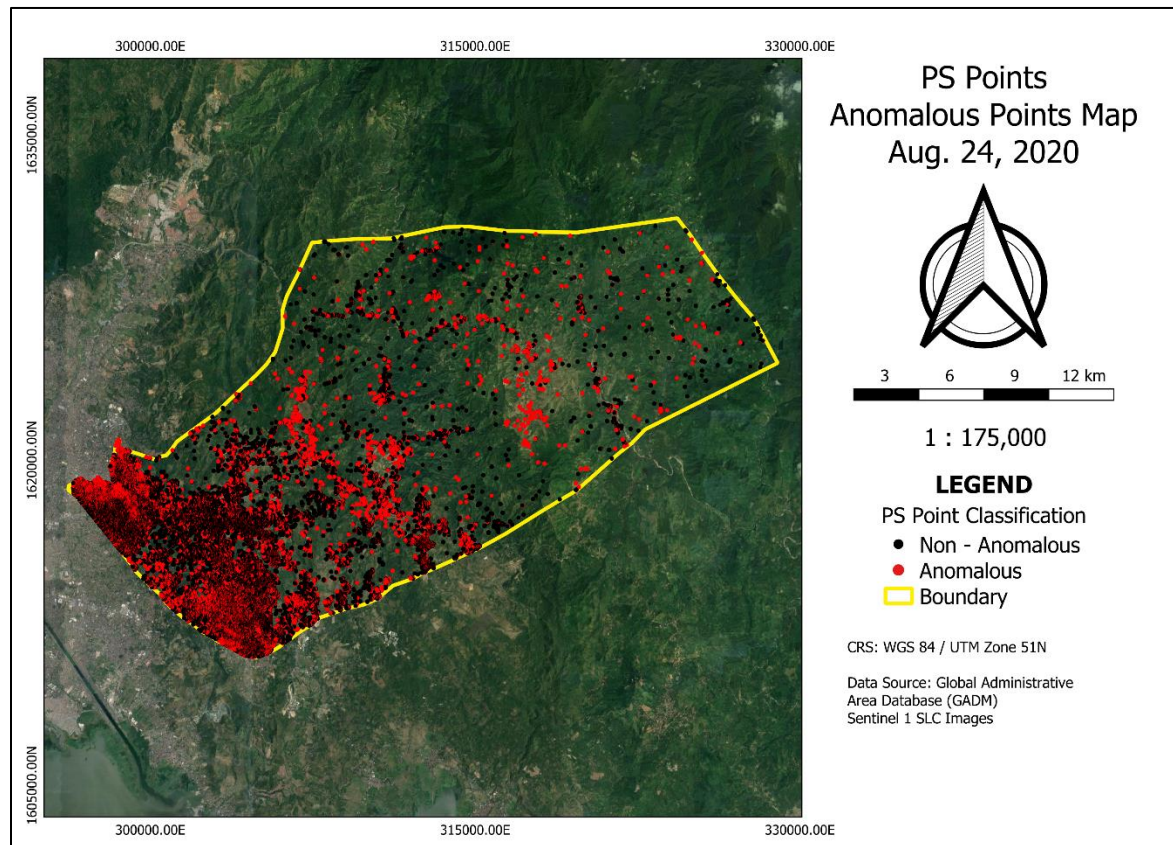

Figure 14. Anomalous Points (24 August 2020)

Figure 14 illustrates the PS points classified as anomalous and non-anomalous for the date of 24 August 2020. The red points in the figure indicate that the movement of those specific points are quicker than the model for those points thus may need for extra attention as these are the movements that may evolve later on to be a pre-failure movement through triggering events. It is important to note that the figure above only classifies points based on relative

movement to the previous 15 displacement measurements. This means that even if the movement is relatively slow and the slope of the graph is near zero, so long as the succeeding point moves beyond the threshold, it will be classified an anomalous point. This is evident in urban areas where movement is not expected to scatter as much therefore the thresholding value computed as the 99% CI becomes smaller due to smaller variations in the displacement measurements used to create the model. For urban settings, this analysis would not give crucial results since there is little variations in the movement therefore the threshold is very low and points can easily exceed the threshold thus classifying it as an anomalous point. This is evident from the figure where there is a significant number of anomalous points in the urban areas in the south western portion of the study area.

The anomalous points depicted in Figure 14 pertain only to the specific date of August 24, 2020. The PS points were classified using the model derived from the initial 15 displacement values spanning from January 21 to August 12, 2020. Subsequently, with each new data acquisition, the model undergoes an updating process. The update involves removing the earliest displacement value in the model and appending the most recent displacement value from the preceding range of data acquisition. At any given point in time, the model comprises a total of 15 measured values, which collectively define the current model. This model update occurs during each acquisition date. Thus, the classification of anomalous points also change dynamically with each new data acquisition.
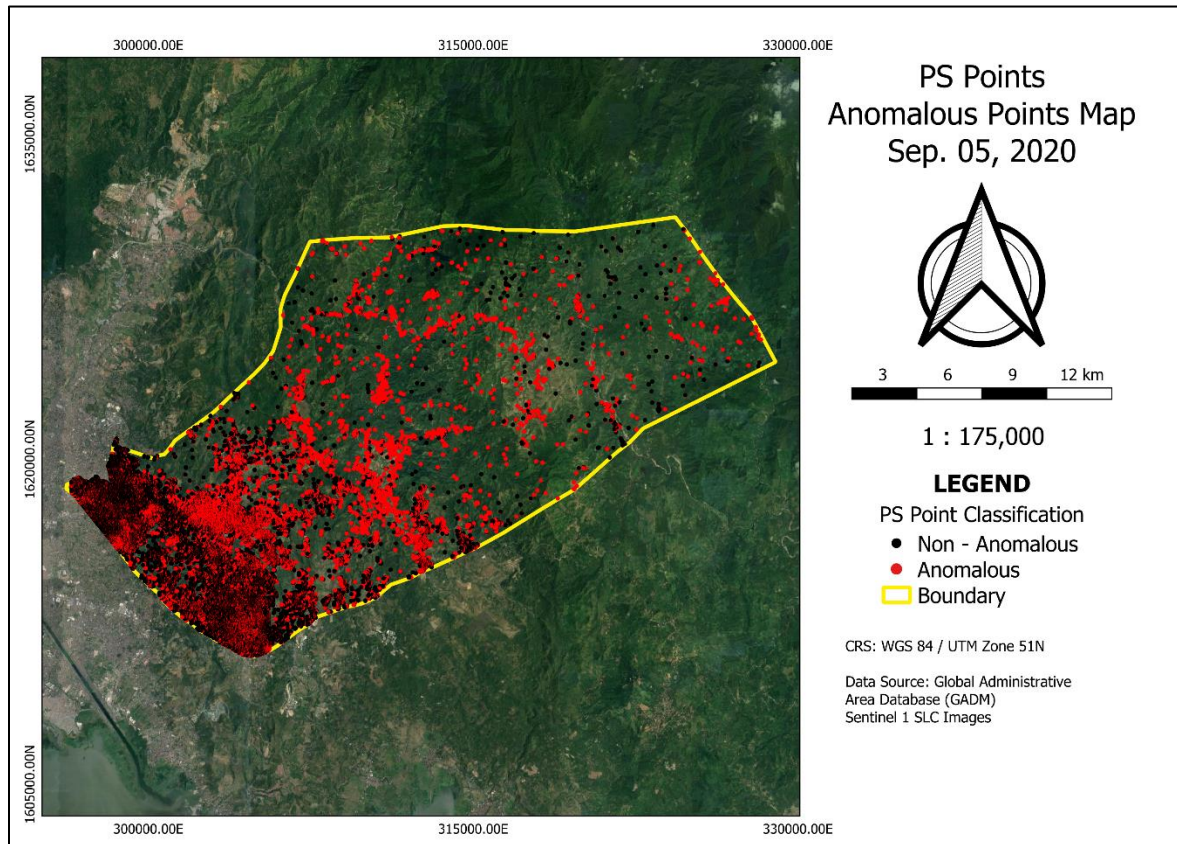

Figure 15. Anomalous Points (05 September 2020)

Using the displacement values of the next set of measurements, a new set of anomalous points are classified. The map showing the anomalous points for the next image acquisition, 05 September 2020, is seen in figure 15. This method is repeated and iterated throughout the entire time frame of the study area.

The continuous process of determining and updating the model, along with the classification of points, provides invaluable insights to local government agencies for prioritizing areas over time. Notably, every 12 days, the model and map can be updated as new SAR images are acquired and added to the image stack for PSI analysis. This constant update of the map highlights the dynamic nature of landslide hazard assessment, revealing where potential pre-failure movements might transition into slope failures.

In addition to the derived velocity data, for each image acquisition, a new spatial layer is generated, serving as a base reference for disaster preparedness. The significance of the anomalous map layer becomes emphasized when integrated with weather forecasts. The most recent and regularly updated anomalous points map pertains to the PS points exhibiting movement behavior that may evolve into slope failures, especially when influenced by significant weather and environmental disturbances. This means that when a significant weather disturbance is expected through forecasting, the local planning agencies may know which areas are most likely to be affected due to the latest behavior of PS points within the vicinity. As a result, local planning agencies gain a potential initial assessment of areas requiring prioritization, facilitating logistical preparations and resource mobilization as needed. This approach enhances and augments the disaster management strategies by focusing on areas at elevated risk of slope failures.

4.4. Landslide Hazard Assessment

In addition to identifying anomalous points, landslide assessment can be conducted by directly examining the displacement measurements of the PS points during the acquisition period. Both the map showing anomalous points and the map displaying displacement values work together to determine not only the classification of the point but also the rate at which the point is moving. This analysis enables the continuous update of both the anomalous points maps and the displacement maps, thus establishing a dynamic landslide hazard assessment tool for local planning agencies. This serves as a basis for continuously refining and updating landslide mitigation measures for each image acquisition period.

Figure 16 shows the displacement of the PS points for 24 August 2020. This goes hand in hand with the map from Figure 14. It can be seen that majority of the urban areas are experiencing little subsidence with magnitude of 0 to 10mm while the mountainous portion on the central rightmost section is experiencing some uplift with magnitudes of 10 to 20mm. The upper central portion, meanwhile, is also experiencing a mix of subsidence and uplift ranging from -10mm to 10mm.
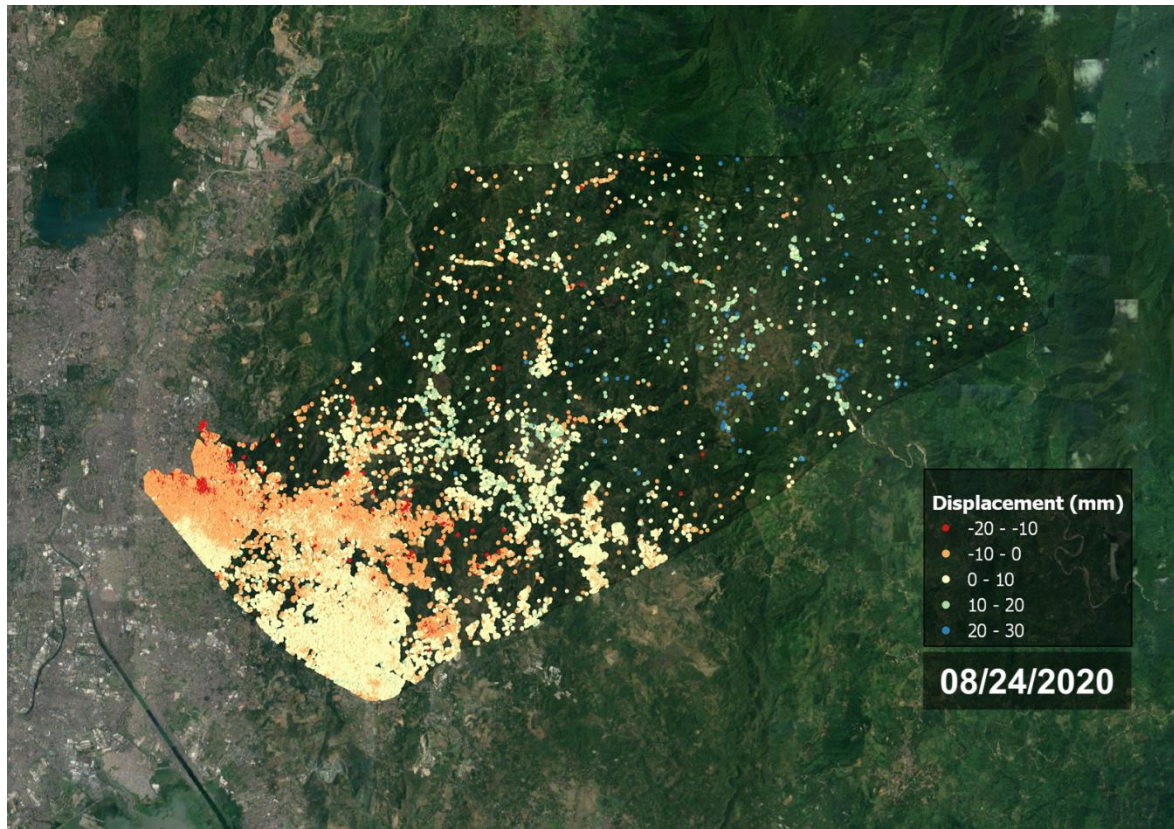
Figure 16. Displacement Map (24 August 2020)

The movements of the PS points within mountainous regions exhibit notable non-uniformity and significant variability. Due to this, the identification of anomalous points becomes crucial. To enhance the integration of the published landslide susceptibility map (see Figure 6) with the outcomes of the PSI processing, it is recommended to overlay the results to derive better insights. The overlay process integrates the susceptibility map with the anomalous points map, providing local planning agencies with an enhanced understanding of which areas are potentially highly susceptible. By combining the susceptibility map with the anomalous points map, local agencies may gain clarity on both the susceptibility classification of specific areas and the actual displacement movements of points within those areas. This integration provides a visual means of identifying points requiring additional attention. Furthermore, it aids in categorizing these points within the context of landslide susceptibility, increasing the overall assessment of landslide risk.
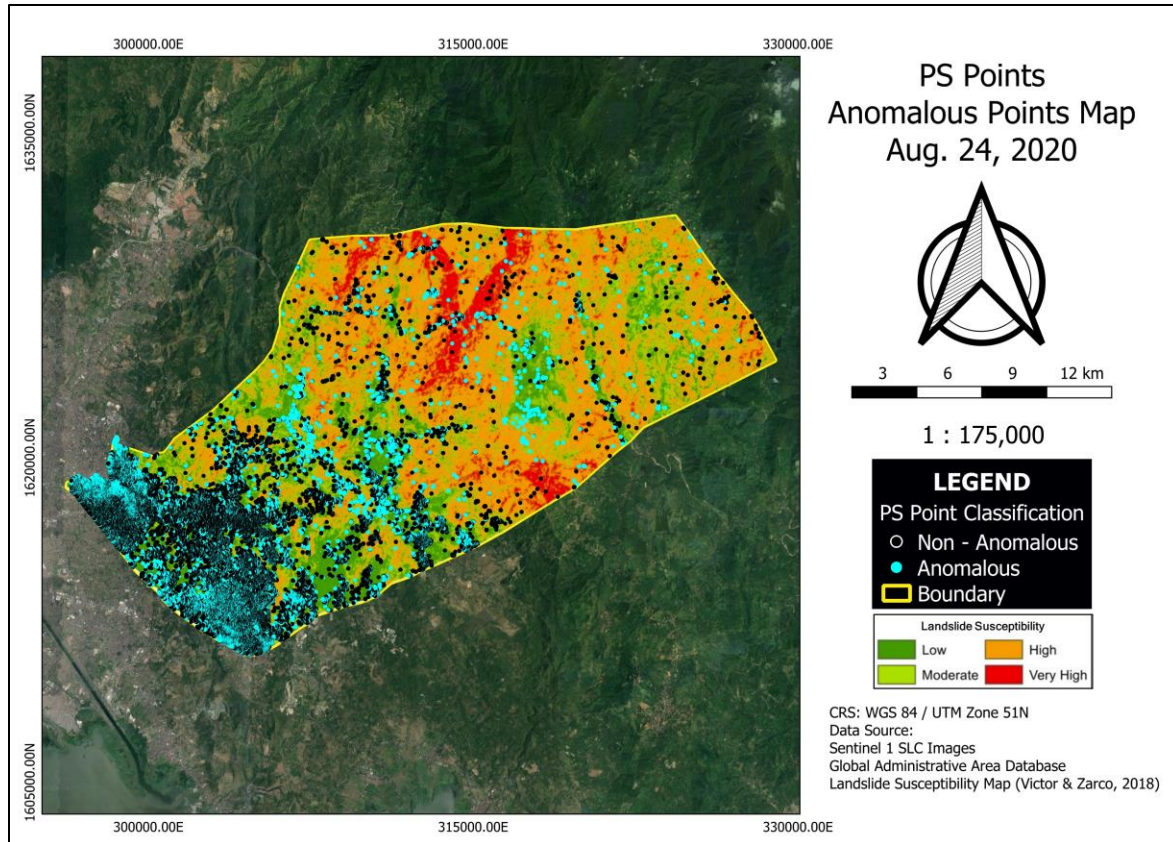
Figure 17. Landslide Susceptibility with Anomalous Points (24 August 2020)

Figure 17 shows the anomalous points from figure 14 overlain with the landslide susceptibility map in figure 6. The combination of these 2 results would give the local government more insights on which areas to focus on for their landslide mitigation measures should a hazard event is anticipated within the acquisition date. From the figure above, it can be seen that there are minimal anomalous points in the central northern most portion corresponding to very high susceptibility and majority of the anomalous points are within the moderate to low classification.

This suggests that on August 24, areas classified as having high landslide susceptibility are less likely to experience slope failures, as the majority of the PS points within these regions are non-anomalous. These points exhibit no significant movement when compared to their behavior during the preceding 15 acquisition dates. Conversely, if a weather bulletin is issued on the said date, the areas to be prioritized should be based on the presence of significant clusters of anomalous points in consideration of their landslide susceptibility. These clusters are anticipated to signify potential pre-failure movements that could evolve into slope failures due to triggering weather events. The same method can be applied to the next set of measurements so that new anomalous points are derived for the next acquisition period. Thus, updating the current combination of landslide susceptibility (see Figure 18).
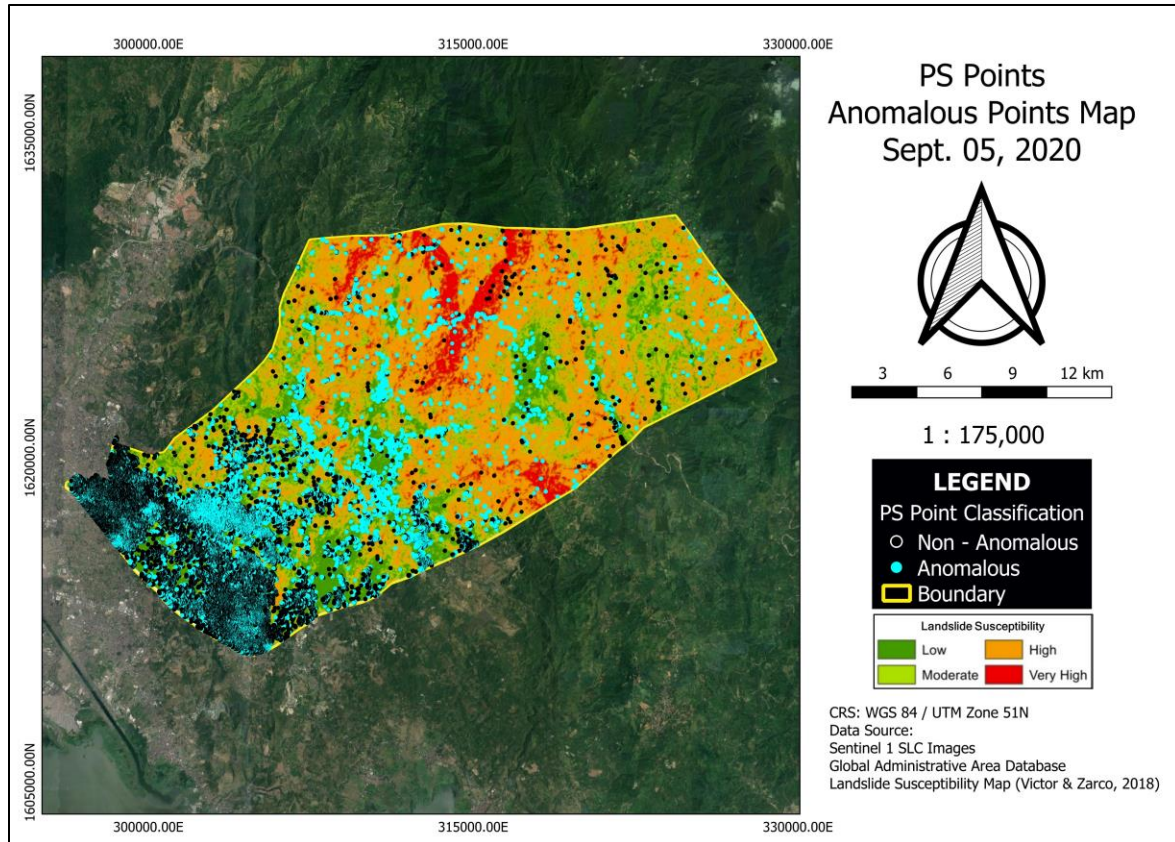
Figure 18. Landslide Susceptibility with Anomalous Points (05 September 2020)

The integration of the published landslide susceptibility map with the results of the PSI analysis yields insights into prioritizing areas for focused attention. This analysis involves examining both the susceptibility classification and the actual displacement measurements for these areas at a specific image acquisition time. The advantage of utilizing PSI for landslide hazard assessment lies in its capability to continuously update maps for a more proactive and dynamic approach to assessing potential landslides.

The published landslide susceptibility map [27] for Antipolo City incorporates a comprehensive list of physical and demographic causative factors to determine landslide susceptibility. A critical layer in this assessment pertains to the actual ground movement of the land. The inclusion of ground movement data, as provided by this study, contributes to the spatial and temporal updatable nature of landslide hazard mapping in the study area.

In this study, an additional layer of information is continually generated, which include the anomalous points and displacement maps. The process spans the entire time frame of the study. With each new image acquisition, the published landslide susceptibility map undergoes updating, receiving 2 new layers in the form of the anomalous points and displacement maps. The integration of the published static map derived from a comprehensive analysis of various causative factors, combined with the two dynamically updatable layers from the PSI analysis, provides essential information for landslide disaster management. This integration comprises

both spatial and temporal dimensions, providing valuable insights for effective hazard mitigation and preparedness for landslide hazards.

The results of this study serve as a valuable supplement to the published landslide susceptibility map of the study area. It provides a spatial layer that can be dynamically updated and integrated into the disaster preparedness and mitigation plans of the local agency. The study's results demonstrate the potential and feasibility of utilizing PSI as a monitoring tool for minute movements in landslide-prone areas, which may signify pre-failure movements that could evolve into slope failures.

It's notable that the data utilized in generating these results is freely available and open-source, ensuring accessibility for all interested in processing and deriving the additional spatial layers for dynamic landslide assessment. However, it's important to note that the application of PSI technology has limitations. In certain regions classified as high susceptibility, there may be a limited number of available PS points, which constrains the extent of hazard analysis in these areas. This limitation is attributed to the phase noise within the resolution cell experienced by individual scatterers, thus, are not detected as candidate PS points in the processing.

4.5 GNSS Displacement Comparison

To validate the results of the displacement measurements obtained through the PSI analysis, the derived values are compared with the displacement values from the GNSS measurements taken at the UP Base Station. Daily GNSS solutions were used to derive displacement measurements. The measurement corresponding to the date of image acquisition was aligned with the GNSS measurement data and plotted against time. In this study, the acquired measurements from GNSS, StaMPS, and SARPROZ are plotted in Figure 19.
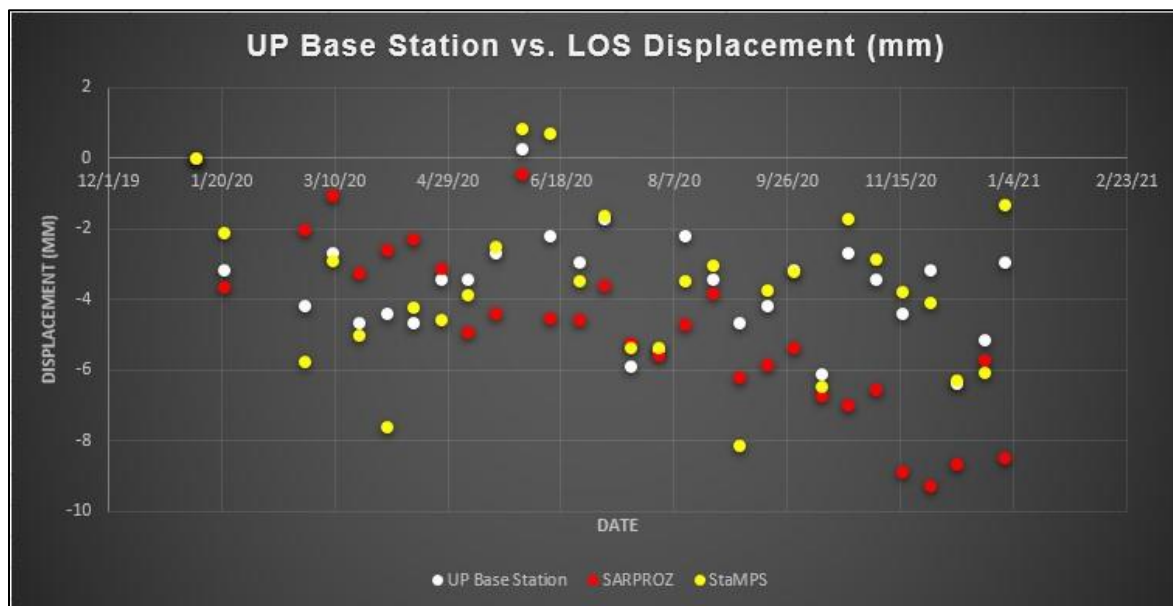

Figure 19. Displacement plot vs UP Base Station

To enable a more effective visualization of the results, a trendline is generated for the three independent measurements, allowing the assessment of the degree of correlation between StaMPS, SARPROZ, and the GNSS measurement. Figure 20 illustrates the trendline for all three measurements.
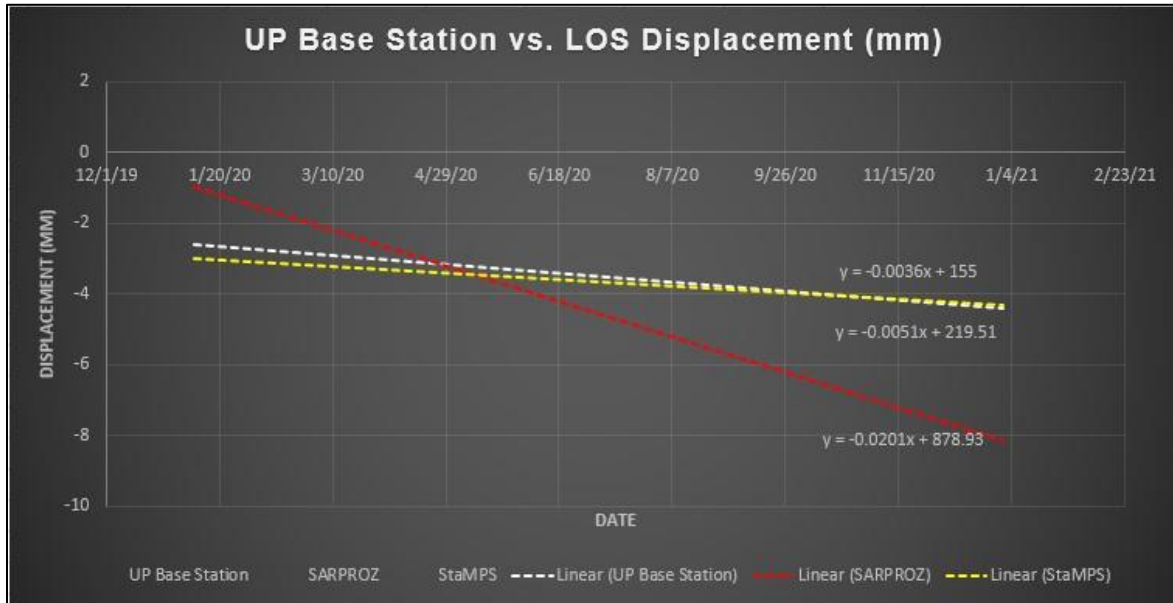

Figure 20. Trendline of Displacement Measurements

Figure 20 depicts the trendline of displacement measurements. It is evident that the measured displacements obtained through SARPROZ overestimated those of the GNSS measurements, displaying an overall trend of subsidence at a significantly faster rate when compared to the GNSS measurements. On the other hand, the displacements derived using StaMPS closely resemble those of the GNSS, with a variation of less than a millimeter. The trendline of the StaMPS measurements closely mirrors the behavior of the GNSS measurements, with only slight differences in slope values.

To quantify the relationship between the measurements, correlation coefficients were computed for both SARPROZ and StaMPS in comparison to the GNSS measurements. A correlation coefficient of 0.61 was calculated for the relationship between SARPROZ and the GNSS, while a strong correlation with a coefficient of 0.83 was determined for StaMPS in relation to the GNSS. These values make it clear that the displacement measurements obtained through StaMPS are more closely aligned with those from the GNSS when compared to SARPROZ. The lower coefficient calculated for SARPROZ is attributed to its tendency to overestimate the subsidence rate, as observed in the slope values of the trendlines. This, along with the detection of a higher number of PS points using StaMPS, presents its applicability as a more viable and reliable method for PSI processing within the study area.

V. CONCLUSION

This study employed PSI techniques to identify ground targets demonstrating stable phase behavior. Two distinct approaches were employed: the temporal model approach using commercial software, SARPROZ, and the spatial correlation approach utilizing the open research package StaMPS. These techniques were applied within a one-year time frame to assess landslide hazards. The process involved the determination of PS points, with resulting derivation of their displacements and velocities for each image acquisition. These PS points play a vital role, particularly in the mountainous regions of the study area, as their measurements provide valuable insights into potential pre-failure movements that could eventually lead to slope failures.

The study included a comparison of SARPROZ and StaMPS to evaluate their suitability for PS point detection in the study area. SARPROZ successfully detected a total of 7,790 PS points, employing a 0.75 SA threshold. On the other hand, StaMPS exhibited greater efficiency by detecting 184,253 PS points using a 0.45 DA threshold. In terms of correlation with GNSS measurements, StaMPS demonstrated a higher correlation coefficient of 0.83. Furthermore, it displayed similar displacement behavior to the GNSS measurements, evident in the trendline slopes of the two measurements.

The study was able to derive the average Line of Sight (LOS) velocity for the PS points within the study area, based on the displacement measurements obtained for each PS point. These velocity measurements, particularly in the mountainous regions, play a crucial role in monitoring potential landslide hazards, as these movements can lead to slope failures. In addition to velocity measurements, the study also identified anomalous points using a 99% CI threshold. It illustrated how these anomalous points changed from one image acquisition to the next. The actual displacements of PS points were also analyzed, providing a comprehensive perspective that was overlaid with the published landslide susceptibility map of the study area to provide additional context for planning and mitigation measures.

Lastly, the use of PSI has demonstrated the potential for dynamic landslide hazard assessment. This approach allows for ongoing updates, providing continuous insights into areas requiring additional attention through the analysis of displacement, velocity, and anomalous points. It is noteworthy that all data used in this study are freely available and open-source, incurring minimal additional costs for the Local Government Unit. Additionally, there is a significant reduction in resource allocation, in both manpower and financial expenses. Also, manpower risk is significantly reduced, as the measurements derived in this study come from space-borne sensors, eliminating the need for deploying personnel in landslide-prone areas.

This study demonstrates the potential of satellite data in supplementing the existing geohazard maps provided by national agencies and published research. It empowers the local government by providing them with the additional information to potentially update their landslide hazard maps on a regular basis and help them in augmenting and supporting their existing resources.

VI. RECOMMENDATION

A key limitation of the study is the ability of the method to detect PS points. Analysis can only be done in areas where PS points are detected. With this, the number and distribution of PS points are crucial. It is recommended to try other PSI approaches to densify the number of PS points in the study area. One method that may be explored for further research is the combination of the PS with Distributed Scatterers (DS). DS are a collection of targets that may not necessarily be represented as a single bright scatterer in a pixel but are close enough for statistical analysis to be done [36]. This can be implemented using the SqueeSAR^{TM} [37] approach or the TomoSAR approach [38]. These approaches combine the use of PS and DS for time series measurements. Another Multi-Temporal InSAR technique such as the Small Baseline Subset (SBAS) InSAR [39] may be explored for sensors with uneven temporal distribution.

While the study successfully detected a high number of PS points in landslide-prone areas, the results are considered experimental as no actual field measurements were conducted in the highly susceptible regions. It is, therefore, recommended to integrate the PSI results with ground movement monitoring sensors to enhance the robustness and reliability of the findings. Specifically, it is suggested to install corner reflectors in areas with a high landslide probability, locations lacking PS points, or areas identified by the LGU as requiring more accurate measurements. These reflectors serve as bright targets, enhancing their detectability as PS points. It is also recommended that GNSS measurements be done for more accurate displacement correlation with ground truth. This can be done via static observation or installation of active geodetic stations for continuous monitoring and measurement validation. Other SAR sensors are also recommended to be used for landslide hazard assessment. More minute movements and higher spatial resolution can be achieved by using an X-band SAR sensor like the TerraSAR X or the COSMO-SkyMed. For areas that are expected to move faster, L band sensors like the NovaSAR are recommended as this has a longer wavelength therefore it can detect faster and more displacement measurements than the C-Band Sentinel 1.

References:
[1]   Cruden D, Varnes D. 1996. Landslide types and processes. In: Turner AK, Schuster RL (eds) Landslides: Investigation and Mitigation, Sp. Rep. 247, Transportation Research Board, National research Council. National Academy Press: Washington DC. p 36–75
[2]   Crozier M, Glade T. 2005. Landslide hazard and risk: Issues, concepts and approach. Landslide Hazard and Risk. John Wiley and Sons Ltd. West Sussex. p. 1–40
[3]   Crozier M. 1989. Landslides: causes, consequences and environment. Routledge, London.
[4]   Hoser T. 2018. Analysing the capabilities and limitations of InSAR using Sentinel-1 data for landslide detection and monitoring. Faculty of Mathematics and Natural Sciences. University of Bonn.
[5]   Skempton H. Hutchinson J. 1969. Stability of natural slopes and embankment foundations, in. Proceedings: 7th. International Conference of Soil Mechanics and Foundation Engineering. State of the Art Volume. Transport; Road Research Laboratory, Mexico. p. 291–340.
[6]   Centre for Research on the Epidemiology of Disasters. 2018. Natural disasters: 2018. Institute Health and Society. Université Catholique de Louvain.

[7]   Philippine Daily Inquirer. 2012. Retrieved from: https://globalnation.inquirer.net/47358/philippines-ranks-3rd-in-landslide-deaths on 09 Mar 2020.

[8]   Rappler. 2018. Retrieved from https://www.rappler.com/newsbreak/iq/212440-list-deadly-landslides-philippines/ on 12 Mar 2020.

[9]   Brabb E. 1993. Proposal for worldwide landslide hazard maps. Proceedings of 7th International Conference and field workshop on landslide in Czech and Slovak Republics. p. 15–27.

[10]   Nikolakopoulos K. et al. 2015. Active landslide monitoring using remote sensing data, GPS measurements and cameras on board UAV. Proceedings Society of Photo-optical Instrumentation Engineers. 9644, 1–9.

[11]   Nikolakopoulos K, et al. 2005. Combined use of remote sensing, GIS and GPS data for landslide mapping. Proceedings. 2005 IEEE International Geoscience and Remote Sensing Symposium. IGARSS '05; Seoul, South Korea. p. 5196-5199. doi: 10.1109/IGARSS.2005.1526855

[12]   Casagli N, et al. 2016. Landslide mapping and monitoring by using radar and optical remote sensing: Examples from the EC-FP7 project SAFER. Remote Sensing Applications: Society and Environment. Elsevier. 4 92-108.

[13]   Richards J, Jia X. 2006. Remote sensing digital image analysis: in introduction. 4th Ed. Springer.

[14]   Woodhouse I. 2005. Introduction to microwave remote sensing. CRC Press.

[15]   Rosen P, et al. 2000. Synthetic aperture radar interferometry. In Proceedings of the IEEE. 88(3):333-382. doi: 10.1109/5.838084

[16]   Takeuchi W. 2014. Wide – area ground deformation analysis using satellite remote sensing. Institute of Industrial Science, The University of Tokyo. Lecture Slides for Fault Evaluation Committee, Japan Society of Civil Engineers

[17]   Ferretti A, Prati C, Rocca F. 2001. Permanent scatterers in SAR interferometry. IEEE Transactions on geoscience and remote sensing. 39(1):8-20.

[18]   Crosseto M, et al. 2015. Persistent scatterer interferometry: a review. ISPRS Journal of Photogrammetry and Remote Sensing. 115: 78 - 89.

[19]   Ferretti A, et al. 2004. InSAR permanent scatterer analysis reveals ups and downs in San Francisco Bay area. EOS, Transactions American Geophysical Union 85.34: 317-324.

[20]   Hooper A. Zebker H. 2007. Phase unwrapping in three dimensions with application to InSAR time series. J. Opt. Soc. Am. A 24:2737-2747.

[21]   Hooper A. 2008. A multi-temporal InSAR method incorporating both persistent scatterer and small baseline approaches. Geophysical Research Letters. 35. doi:10.1029/2008GL034654

[22]   Jia H, et al. 2019. Landslide deformation monitoring by adaptive distributed scatterer interferometric synthetic aperture radar. Remote Sens. 11: 2273. doi:10.3390/rs11192273

[23]   Perissin, D, et. al. 2011. SARPROZ InSAR tool for urban subsidence/manmade structure stability monitoring in China. Proc. of ISRSE. Sydney, Australia.

[24]   Hooper A. 2011. Recent advances in SAR interferometry time series analysis for measuring crustal deformation. Tectonophysics. Elsevier. 514 – 517:1 – 13.

[25]   Morales E, et. al. 2001. The Cherry Hills landslide tragedy. The 2nd Civil Engineering Conference in the Asian Region, Tokyo.

[26]   Philippine Star. 2009. Retrieved from https://www.philstar.com/headlines/2009/09/29/509268/floods-landslides-worsening-antipolo on 09 March 2020.

[27]   Victor J, Zarco M. 2018. Multivariate logistic regression approach for landslide susceptibility assessment of Antipolo, Rizal. Philippine Engineering Journal. 39(2):27-40.

[28]   European Space Agency. 2020. Retrieved https://rus.copernicus.eu/portal/the-rus-library/learn-by-yourself.

[29]   Foumelis M, et al. 2018. SNAP - StaMPS integrated processing for Sentinel-1 persistent scatterer interferometry. In Geoscience and Remote Sensing Symposium (IGARSS). IEEE International, IEE

[30]   Hooper A, et al. 2004. A new method for measuring deformation on volcanoes and other natural terrains using InSAR persistent scatterers, Geophys. Res. Lett., 31:L23611. doi:10.1029/2004GL021737

[31]   Minh D. 2021. Ground motion from space. Vietnam Space Center. October 15, 2021.

[32]   Qin Y. 2018. Exercise 3: Pixel tracking with SARPROZ in a toy example. SARPROZ processing tutorial series.

[33]   Khorrami M, et al. 2020. Extreme subsidence in a populated city (Mashhad) detected by PSInSAR considering groundwater withdrawal and geothermal properties. Sci Rep. Jul 9-10(1):11357.

[34]   Nationwide Operational Assessment of Hazards. n.d. Retrieved from https://noah.up.edu.ph/know-your-hazards/landslide on 13 April 2021.

[35]   Morales E, et al. 2001. The Cherry Hills landslide tragedy. 2nd Civil Engineering Conference in the Asian Region. Tokyo.

[36]   Jia H, et al. 2019. Landslide deformation monitoring by adaptive distributed scatterer interferometric synthetic aperture radar. MDPI. Remote Sens. 11:2273 doi:10.3390/rs11192273

[37]   Ferretti A, et al. 2011. A new algorithm for processing interferometric data-stacks: SqueeSAR. IEEE Transactions on Geoscience and Remote Sensing. 49(9):3460-3470. doi: 10.1109/TGRS.2011.2124465

[38]   Minh D. Ngo YH. 2022. Compressed SAR interferometry in the big data era. Remote Sens. 14:390. https://doi.org/10.3390/rs14020390

[39]   Li S, et al. 2022. Review of the SBAS InSAR Time-series algorithms, applications, and challenges. Geodesy and Geodynamics. 13(2). https://doi.org/10.1016/j.geog.2021.09.007

[40]   Barra A, et al. 2016. First insights on the potential of Sentinel-1 for landslides detection. Geomatics, Natural Hazards and Risk. 7(6): 1874-1883 http://dx.doi.org/10.1080/19475705.2016.1171258

[41]   Aslan G, et al. 2020. Landslide mapping and monitoring using persistent scatterer interferometry (PSI) technique in the French Alps. Remote Sens. 12:1305. doi:10.3390/rs12081305

[42]   Sara F, et al. 2013. Landslide inventory updating by means of persistent scatterer interferometry (PSI): The Setta Basin (Italy) case study. Geomatics, Natural Hazards and Risk. 6(5–7):419–438 http://dx.doi.org/10.1080/19475705.2013.866985

[43]   Liu X, et al. 2018. Multi-temporal Loess Landslide inventory mapping with C-, X-and L-band SAR datasets—A case study of Heifangtai Loess Landslides, China. Remote Sens. 10:1756.